International Symposium
On Turbulence and Shear Flow
Phenomena (TSFP-8)
August 28 - 30, 2013 Poitiers, France

CHARACTERIZATION OF STRUCTURES ASSOCIATED WITH LOW- AND HIGH-SHEAR REGIONS IN EXPERIMENTAL AND NUMERICAL TURBULENT CHANNEL FLOWS

Omid Amili[1]
omid.amili@monash.edu

Yoshinori Mizuno[2]
ymizuno@mail.doshisha.ac.jp

Nicolas Buchmann[1]
nicolas.buchmann@monash.edu

Callum Atkinson[1]
callum.atkinson@monash.edu

Julio Soria [1,3]
julio.soria@monash.edu

[1] Laboratory for Turbulence Research in Aerospace and Combustion (LTRAC),
Department of Mechanical and Aerospace Engineering, Monash University, Australia
[2] Department of Mechanical and Systems Engineering, Doshisha University, Japan
[3] Department of Aeronautical Engineering, King Abdulaziz University,
Jeddah, Kingdom of Saudi Arabia

ABSTRACT

Measurements of the wall shear stress distribution in a fully developed turbulent channel flow have been performed using a film-based sensor. The sensor, as a direct method for measuring the wall shear stress, enables the conduction of measurements in a relatively large domain with high spatial resolution. From the experimental data, instantaneous velocity components in the region of $y^+ \lesssim 5$ were approximated using the instantaneous wall shear stress distribution, the application of the continuity condition, and Taylor expansion of the velocity at the wall. In addition, a direct numerical simulation of a turbulent channel flow at the same Reynolds number range was used to assess the experimental results and to extend the analysis to the buffer layer. The investigated Reynolds numbers are in the range of 2,100-2,900 based on the friction velocity and the half channel height. The distribution of the fluctuating wall shear stress reveals the presence of low- and high-shear regions oriented in the streamwise direction. This indicates the imprint of existing streaky structures in the near-wall region. The conditionally averaged field of low-shear stress regions exhibits the existence of a counter-rotating vortex pattern elongated in the streamwise direction. The averaged map conjectures the signature of long quasi-streamwise vortices or stretched legs of hairpins as the dominant structures in the immediate vicinity of the wall.

INTRODUCTION

Coherent streaks have been widely investigated since their early identification in the flow visualizations by Hama (1954), and Kline *et al.* (1967). Streaks as a universal feature of wall-bounded turbulent flows play an important role in the turbulence generation process. The experimental characterization of these coherent structures which dominant the viscous and buffer layers is a difficult task due to the relatively small size of the region. To the best of authors' knowledge, the first volumetric experimental examination of instantaneous flow structures in the viscous/buffer layer became available by Sheng *et al.* (2009). The technique used in the mentioned study benefits from high accuracy and high spatial resolution. However, the sample size is relatively small and the field of view is probably too limited to capture streaks even in the spanwise direction. An alternative approach is the measurement of the wall shear stress distribution and estimation of the velocity field using a Taylor expansion as is used here. The two-dimensional measurement of the instantaneous wall shear stress field allows the computation of all three components of the velocity field in the immediate vicinity of the wall. The present study is aimed at reconstructing the instantaneous velocity field and identifying the dominant stress and flow patterns. The footprint of the near-wall coherent structures on the wall are identified using the conditional averages of the wall shear stress fields under different specified conditions. The methodology, experimental, and numerical datasets are briefly addressed.

METHODOLOGY

The viscous layer is characterised by a length scale that is proportional to yu_τ/ν and a time scale which is proportional to the wall unit of time, ν/u_τ^2. The wall distance and the fluid's kinematic viscosity are shown with y and ν respectively. u_τ is the friction velocity and is defined by the mean wall shear stress, $\overline{\tau_w}$, and the fluid density, ρ, as $u_\tau = \sqrt{\overline{\tau_w}/\rho}$. The most distinguishable feature of this layer is its ability to adjust most rapidly to changes in wall conditions. As a result, it is the most appropriate part of the turbulent boundary layer to infer wall conditions and con-

sequently it is suitable to determine the instantaneous wall shear stress (Haritonidis, 1989). On the other hand, upon direct measurement of the instantaneous wall shear stress using no assumption for the flow field, the instantaneous velocity can be computed.

In this region, the absolute magnitudes of velocity fluctuations tend to zero as the wall is approached. However, the local turbulent level of the streamwise component of the velocity, u'/U, asymptotes to a maximum and constant value. Similarly, the local turbulent level of the spanwise velocity, w'/U, approaches to a maximum value in this region. Thus, these fluctuations make the region the most turbulent portion of the boundary layer. It can be easily shown that the asymptotes of the turbulent intensities of the streamwise and spanwise velocity components are associated with the corresponding mean and fluctuating wall shear stress components.

Using the first-order Taylor expansion of the velocity around a point located at the wall, i.e. y=0, the streamwise and spanwise velocity components can be written as follows:

$$u = \frac{\partial u}{\partial y}\Big|_{y=0} y = \frac{\partial u}{\partial y} y = \frac{\tau_x}{\mu} y \tag{1}$$

$$w = \frac{\partial w}{\partial y}\Big|_{y=0} y = \frac{\partial w}{\partial y} y = \frac{\tau_z}{\mu} y \tag{2}$$

where τ_x and τ_z are the wall shear stress components in the streamwise and spanwise directions respectively. By employing a second-order central difference scheme, the in-plane velocity gradients, $\partial/\partial x$ and $\partial/\partial z$, for the streamwise and spanwise velocity components are calculated. Then, by using the continuity equation, the wall-normal gradient of the wall-normal velocity is obtained:

$$\frac{\partial v}{\partial y} = -\frac{\partial u}{\partial x} - \frac{\partial w}{\partial z} \tag{3}$$

Using this gradient component, the wall-normal velocity component can be retrieved as a second-order approximation:

$$v = -\frac{1}{\mu}\left(\frac{\partial \tau_x}{\partial x} + \frac{\partial \tau_z}{\partial z}\right)\frac{y^2}{2} \tag{4}$$

As a result, all three velocity components can be computed by having the instantaneous wall shear stress distribution. For this purpose, a certain distance from the wall is selected. This distance should be located in the viscous layer to satisfy the linearity requirement, i.e. $y^+ \lesssim 5$. The results based on this analysis are going to be compared with a turbulent channel flow DNS with the Reynolds number in the range of the experimental condition. Hence, similar heights to the DNS database have been chosen to reconstruct the velocity components. The first plane from the wall corresponds to $y^+ \approx 0.06$.

The reconstruction quality using the experimentally measured wall shear stress described in the following section was evaluated using the DNS turbulent channel flow database addressed in the DNS DATA SET section. The comparative analysis shows that this approach enables the calculation of the instantaneous velocity profiles within the viscous sublayer. The expected value of the difference between the experimental and numerical velocity fields increases with the wall distance. The largest deviation is found for the streamwise velocity component reaching approximately 0.25 wall units equivalent to $\sim$5% of the local mean velocity at the upper limit of the viscous region.

EXPERIMENTAL DATA SET

Measurements have been performed in the wind tunnel facility located in the Laboratory for Turbulence Research in Aerospace and Combustion (LTRAC) at Monash University. The measurement of the instantaneous wall shear stress is based on the development and application of a film-based shear stress sensor. The detailed design of the sensor and its characteristics has been described in detail in Amili & Soria (2011). Here, only a very brief overview is provided. An elastic film of known geometry and mechanical properties is flush mounted at the lower wall of the test section. The local deformation of the film is proportional to the local shear load applied by the flow. An optical technique is used to measure the film deformation caused by the flow field. For this purpose, the film is imaged at the flow-off and flow-on states and then multi-grid cross-correlation digital particle image velocimetry is used to measure the tangential deformation with high sub-pixel accuracy.

The channel flow facility has a working section with the length of 4.6 m and the width of 1 m with the width to height ratio of 9.75:1. A film with the shear modulus of 84 Pa and the thickness of 1 mm was used as the shear stress sensor in the present work. It was mounted approximately 41 channel height downstream of the test section entrance where the flow is fully developed turbulent. The calibration of the sensor indicates the linear elastic solid behaviour of the homogeneous and isotropic film. Frequency response of the film is a low-pass filter with the bandwidth of 160 Hz based on the -3 dB point in the sensor gain. The spatial resolution of the measurements is approximately 216 μm corresponding to 9$\sim$12 wall units. Experiments were carried out at six Reynolds numbers in the range of 2,100$-$2,900 based on the friction velocity and the half channel height, $Re_\tau = u_\tau(H/2)/\nu$. In the present study, the Re_τ=2,830 data set is used. However, results in other experimental sets are fairly similar to the ones shown here. For a detailed description of the facility, flow characteristics, wall shear stress sensor, governing equations, manufacturing process, calibration, and the accuracy assessment, the reader is referred to Amili (2012).

DNS DATA SET

In order to assess the experimental results, and also to extend the analysis to the buffer layer, a direct numerical simulation of an incompressible turbulent channel flow at the Reynolds number of $Re_\tau \approx 2,300$ is used. This high fidelity simulation enables the comparison of the experimental data with a similar flow type of DNS within the range of the experimentally investigated Reynolds numbers. The turbulent channel flow was simulated by solving the incompressible Navier-Stokes equations for the primitive variables using methods similar to that described in Simens *et al.* (2009). The number of grid points in the streamwise, wall-normal, and spanwise directions are $N_x = 3,072$,

$N_y = 1,441$, and $N_z = 3,072$ respectively. The corresponding spatial resolutions are $\Delta x^+ = 9.4$, $\Delta y^+_{max} = 4.3$, and $\Delta z^+ = 4.7$. The size of the computational box in the streamwise, wall-normal, and spanwise directions is $L_x = 4\pi h$, $L_y = 2h$, and $L_z = 2\pi h$ respectively where h is the half channel height. For further details regarding the database, see Mizuno *et al.* (2011).

RESULTS

The visual inspection of the wall shear stress fields shows the signature of flow structures in the vicinity of the wall. An example of the instantaneous wall shear stress and the corresponding reconstructed velocity field is shown in Figure 1. The presence of low- and high-shear regions aligned in the streamwise direction indicates the streaky nature of structures in the extreme vicinity of the wall.

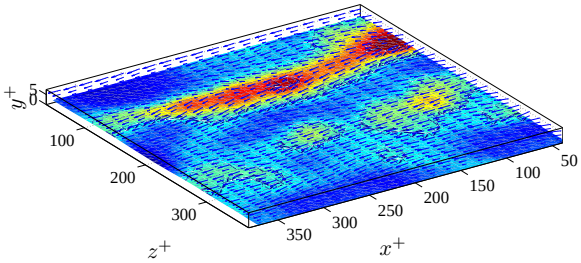

Figure 1. A sample sub-region of the reconstructed instantaneous velocity field in the viscous layer. Every second vector in each direction is shown. The contour represents the normalized streamwise wall shear stress distribution, $\tau_x / < \tau_x >$, from 0.6 (dark blue) to 1.5 (dark red).

An example of the instantaneous wall shear stress field and its corresponding wall-normal velocity component is shown in Figure 2. The contour shows the distribution of the streamwise wall shear stress normalized by the mean stress. The iso-surfaces represent the reconstructed wall-normal velocity component within the viscous layer. Elongated regions with upward and downward wall-normal velocity just above the low-shear streaks (shown in dark gray) can be observed.

Conditional average in low-shear regions

In order to reveal the dominant structure associated with regions of local minimum and maximum wall shear stress, conditional averaging is employed. Figure 3 shows an example of the local wall shear stress field in the low-shear region. In the conditional averaging process, events with the shear stress of $\tau'_x / < \tau_x > \leq -0.2$ are specified to find the pattern associated with the local low wall shear stress. The following averaging procedure suggested by Bakewell & Lumley (1967) and applied by Sheng *et al.* (2009) is used to find the average of the wall shear stress pattern:

$$< \tau'(\Delta x, \Delta z) >_{\tau'_{x,min}} = \left\langle \tau'(x - x_m, z - z_m) \mid \tau'_x \leq -0.2 < \tau_x > \right. \\ \left. \& \quad \tau'_{x,min} = \tau'_x(x_m, z_m) \right\rangle \qquad (5)$$

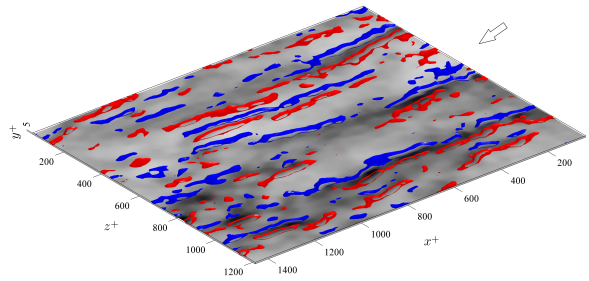

Figure 2. A sample instantaneous wall shear stress distribution. The contour represents $\tau_x / < \tau_x >$ from 0.6 (dark gray) to 1.5 (light gray). The reconstructed wall-normal velocity component within $0 \lesssim y^+ \lesssim 5$ is shown with blue (upward) and red (downward) iso-surfaces.

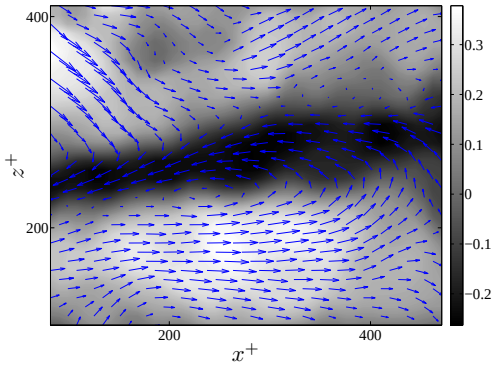

Figure 3. Fluctuating wall shear stress pattern in a low-shear region colored by the normalized streamwise fluctuation, $\tau'_x / < \tau_x >$. The flow direction is from left to right.

where x and z are the coordinates in the streamwise and spanwise directions and x_m and z_m are the coordinates where the extremum of wall shear stress occurs. The angle brackets indicate ensemble average and the brackets with the subscript show the conditional average under the specified condition. The magnitude of the selected threshold level is small enough to have sufficient number of fields to contribute to the average field and is large enough to represent the low-shear events. The probability density function of the wall shear stress fluctuations was used as a guide for this purpose. In the averaging procedure, the local minima of the low-shear region is translated to the origin of the averaged field. In Equation 5, the fluctuating wall shear stress distribution at the determined condition is calculated. In the same way, at the specified event, other variables including the wall-normal vorticity, ω_y, and the wall-normal velocity, u_y, are conditionally averaged.

In Figure 4, the conditional average of the wall shear stress distribution in low-shear regions is presented. Negative streamwise fluctuations along the centerline of the averaged field are accompanied by positive fluctuations on both sides. The averaged vector field of the fluctuating wall shear stress shown in Figure 4(a) reflects a converging stress pattern near the central region. This indicates that in regions with low wall shear stress, the magnitude of the spanwise component relative to the streamwise component increases. The map reveals the signature of a pair of long counter-

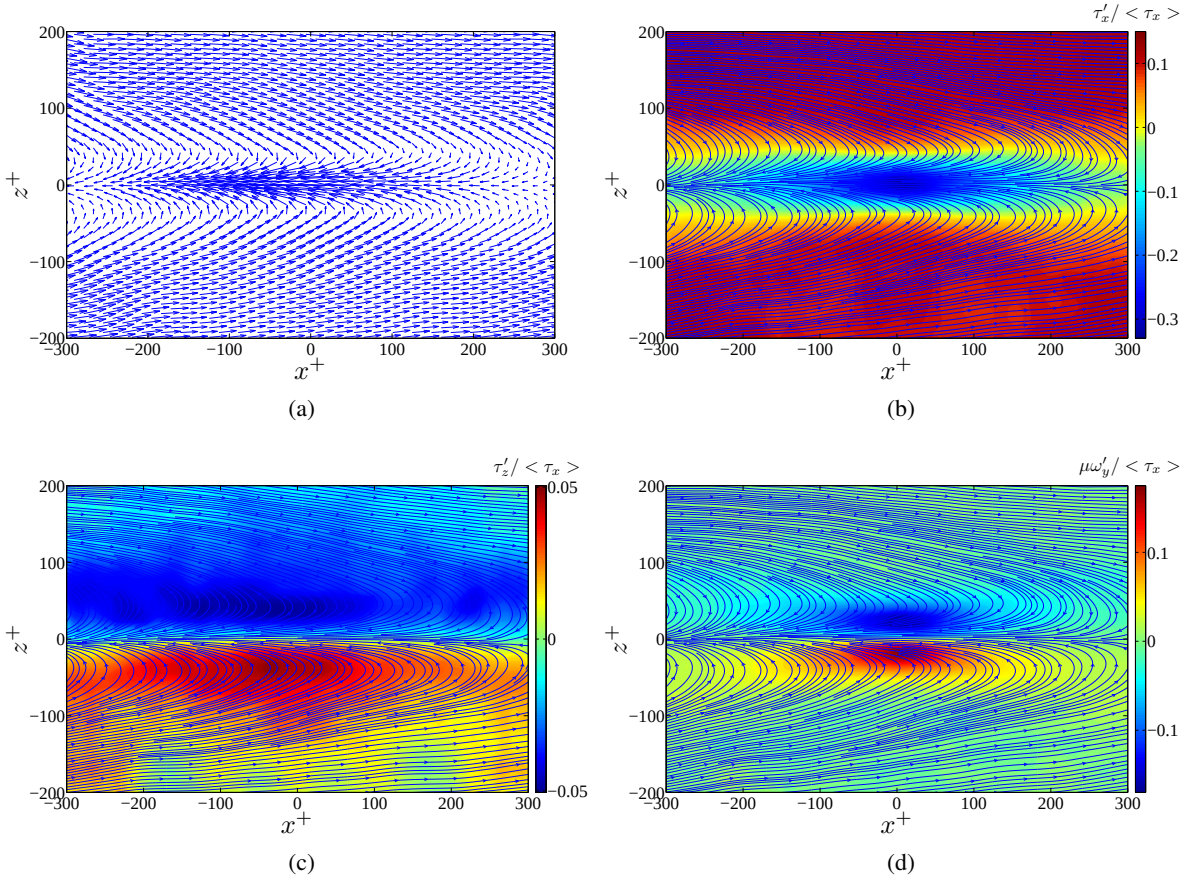

Figure 4. The conditionally averaged wall shear stress pattern with local low-shear stress. The specified events are in the range of $\tau_x'/ < \tau_x > \leq -0.2$. (a) fluctuating wall shear stress vector field; (c) streamwise wall shear stress; (d) spanwise wall shear stress; (e) wall-normal vorticity. The flow direction is from left to right and lines in figures (b) to (d) show the fluctuating streamlines at the wall.

rotating vortices aligned in the streamwise direction. Note that the symmetry observed in the conditional average fields is due to the statistical symmetry of the flow and the type of the specified condition. As inferred from the instantaneous wall shear stress fields, including the one showed in Figure 3, individual shear stress patterns may be asymmetric and meandering.

Figure 4(b) shows the normalised streamwise stress fluctuations. The reduced wall shear stress region along the central area of the averaged field closely resembles the elongation of the two-point correlation map shown in Amili (2012). The spanwise extension of the decreased wall shear stress region estimated from the conditional averaged field is approximately 80 ℓ^+ which shows fairly good consistency with the width calculated from the two-point correlation profile. The spanwise component of the fluctuating wall shear stress is provided in Figure 4(c). Again, this map clearly displays the increase of the spanwise wall shear stress as the distance towards the low-shear region decreases. It shows how the spanwise component accompanies the streamwise component to form the low-shear stress in the streamwise direction.

The rotational patterns on the wall along the reduced shear region are more evident in the plot of the wall-normal vorticity shown in Figure 4(d). The positive (counter-clockwise) and the negative (clockwise) wall-normal vorticities are illustrated with red and blue cores respectively. This is an indication of the presence of quasi-streamwise vortices or stretched legs of hairpins in the vicinity of the wall. A comparison between Figures 4(b) and 4(d) shows that the low-shear region is surrounded by negative wall-normal vorticity values on the top and positive values on the bottom. Such structures induce backward flow and consequently leave negative shear stress fluctuations on the wall.

The conditional averaged field of low-shear events shown here bears close similarities with the wall shear stress pattern reported by Grosse & Schröder (2009). Tomkins & Adrian (2003) also noticed the signature of hairpin vortices in the streamwise-spanwise planes in a turbulent boundary layer at different heights from the wall. Their PIV experiments revealed the elliptical counter-rotating vortex patterns near the low-speed streaks. An observation of that study is that as the distance from the wall decreases, the elliptical pattern becomes more elongated in the streamwise direction. This is consistent with the pattern of wall shear stress observed in the current study. An explanation is that the inclination angle of hairpin vortices with respect to the wall reduces as the wall distance decreases. Hence, the lower hairpin legs remain longer along the streamwise direction which their footprints on the wall have been measured here. In Tomkins & Adrian (2003), the authors observed elongated elliptical shapes in the conditional eddy pattern at $y^+ = 21$ as an indication of existence of vortices at a small angle relative to the wall.

On the other hand, Sheng *et al.* (2009) based on the measurements in the buffer layer of a turbulent duct flow

reported counter-rotating quasi-streamwise vortices with equal circulation strength in the immediate neighbourhood of the low stress region. The lifted vortex lines with the Ω-shape heads just above the decreased shear region shows the relation of ejection events with the low-shear stress. However, the inclination angle of the averaged vortex pairs reported in the mentioned study is more than 45^o and the elongation of low-shear region in the streamwise direction is shorter than that of the present measurement and the length scale usually reported in the literature.

The converging pattern of the velocity is also evident in the conditionally averaged field of low-shear regions obtained from the DNS turbulent channel flow shown in Figure 5. The low-shear stress region is shown by dark gray and the iso-surfaces represent the upward flow (blue) and and downward flow (red) in the neighbourhood of the low-shear region. The ejection event above the low-shear region is the dominant flow structure.

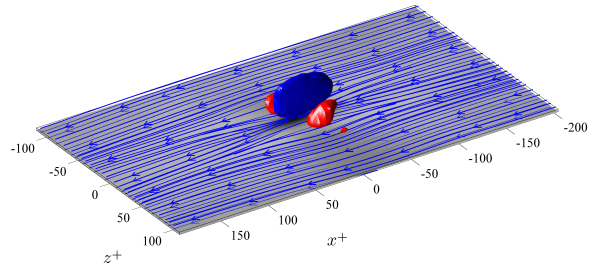

Figure 5. The conditionally averaged wall shear stress pattern in the low-shear stress region ($\tau_x'/ < \tau_x > \leq -0.2$) computed from the DNS turbulent channel flow described earlier. The blue iso-surface shows positive wall-normal velocities accompanied by weaker negative wall-normal velocities shown by red iso-surfaces.

Conditional average in high-shear regions

The conditional averages of the wall shear stress fields at high-shear regions based on the condition of $\tau_x'/ < \tau_x > \geq 0.2$ are presented in Figure 6. A procedure similar to the relation described earlier is used to find events with high-shear stress fluctuations.

The divergence pattern of the wall stress in the central region of the conditional averages can be clearly observed in the average fields of the fluctuating wall shear stresses shown in Figure 6. The elongated high-shear region in the streamwise direction is the dominant stress pattern. The streamwise component of the wall shear stress shown in Figure 6(b) remains relatively high along the centerline of the averaged field but decays rapidly in the spanwise direction. On the other hand, the spanwise component of the wall shear stress increases from zero as the distance from the centerline increases (see Figure 6c). The spanwise wall stress is due to the rotational patterns with similar strength but opposite signs on both sides of the centerline. This creates a diverging distribution of wall shear stress away from the central region which is quite clear in the pattern of the skin friction lines. A similar flow pattern exists in the immediate vicinity of the wall of which its signature on the surface is the generation of this lateral stress distribution. The movement of the fluid away from the centerline causes the flow in the central region to accelerate and consequently to increase the wall shear stress. The vorticity map shown in Figure 6(d) is an indication of such a flow pattern described above. As pointed out previously, individual stress regions which contribute to the conditional averages are not necessarily symmetric. The conditional average of high-shear regions described here shares clear similarities with the one provided by Sheng *et al.* (2009). However, in the noted study, two long but weak low-shear stress streaks are also observed on sides of the high-shear stress region.

CONCLUDING REMARKS

Based on the experimental methodology addressed in this work, instantaneous wall shear stress fields in a turbulent channel flow have been measured with high spatial resolution. The two-dimensional measurements indicate the co-occurrence of regions of low- and high-shear stress which are mostly aligned in the streamwise direction. To provide statistical support and quantify the spatial coherence of these patterns, conditional averages of the fluctuating wall shear stress components at certain conditions were provided.

The conditional average of regions with low-shear stress in the streamwise direction with the determined condition of $\tau_x'/ < \tau_x > \leq -0.2$ clearly shows an elongated counter-rotating vortex pattern on the wall. The elongated length of the low-shear region showed in Figure 4(a) is an indication of the persistence of the streaky features along the streamwise direction. The mean width of the low-shear regions is approximately 80 ℓ^+ which is in very good agreement with the data available in the literature. According to the streamlines on the surface and the corresponding wall-normal motions, flow structures which are responsible for the large and negative wall shear stress fluctuations are estimated as:

* counter-rotating quasi-streamwise vortices with small inclination angle with respect to the wall, and
* stretched legs of hairpins in the immediate vicinity of the wall.

A pair of counter-rotating vortices with similar strength but opposite signs or the lower parts of the hairpin legs induce negative wall shear stress fluctuations in the streamwise direction and generate ejection motions between them. This pattern of elongated wall-normal component of vorticity is also clear in the instantaneous snapshots (e.g. Figure 2). Such turbulent structures in the immediate vicinity of the wall are elongated and nearly streamwise. This finding is consistent with the observation of Grosse & Schröder (2009), and shows considerable similarities with the structures measured by Tomkins & Adrian (2003).

In addition, the conditional average of events with the specified condition of $\tau_x'/ < \tau_x > \geq 0.2$ reveals a diverging distribution of high wall shear stress fluctuations similar to the map provided by Sheng *et al.* (2009). This suggests that the dominant flow structures associated with the high streamwise wall shear stress fluctuations possess higher spanwise velocity that cause acceleration of the fluid elements along the streamwise direction.

ACKNOWLEDGMENT

The financial support to perform this research by the Australian Research Council is gratefully acknowl-

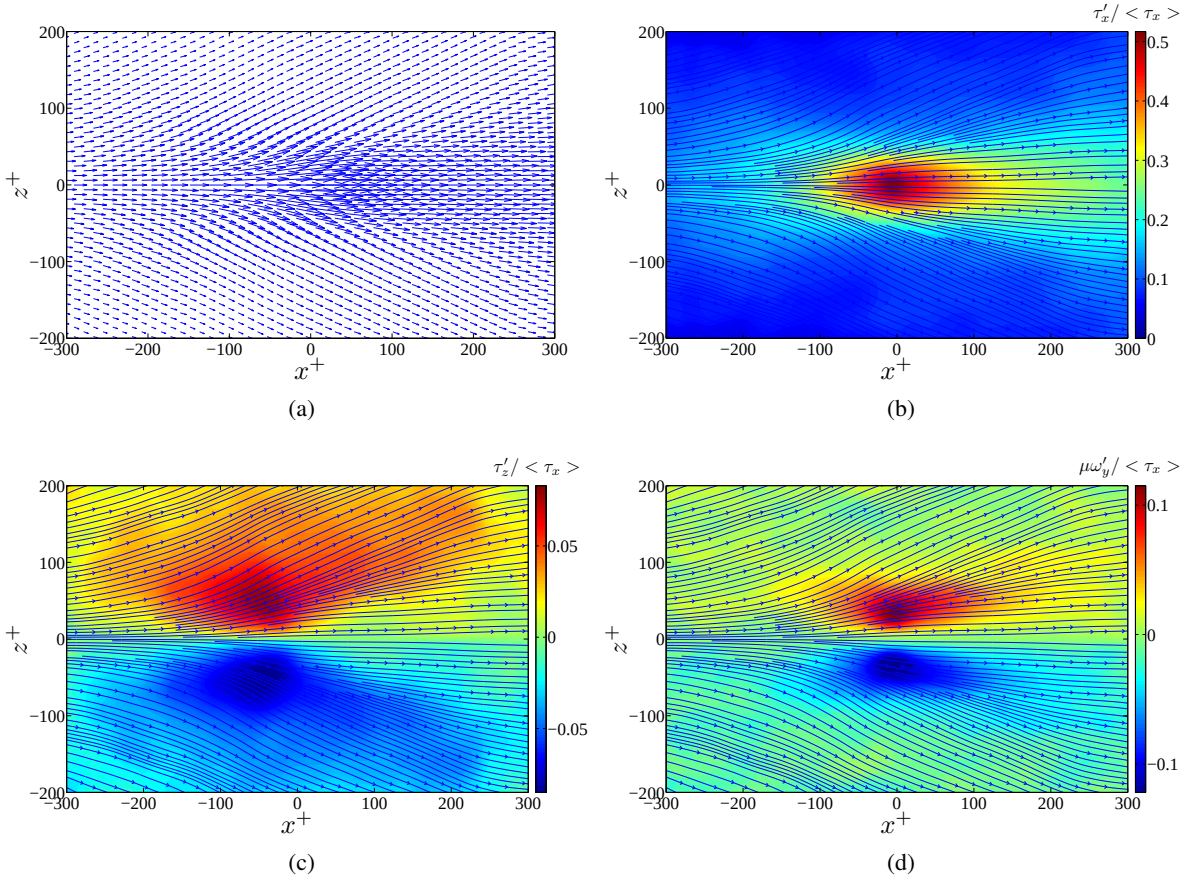

Figure 6. The conditionally averaged wall shear stress patterns with the determined condition of $\tau_x'/ < \tau_x > \geq 0.2$. (a) fluctuating wall shear stress vector field; (b) streamwise wall shear stress; (c) spanwise wall shear stress; (d) wall-normal vorticity. The flow direction is from left to right and lines in figures (b) to (d) represent the fluctuating skin friction lines.

edged. This research was undertaken with the assistance of resources provided at the National Computational Infrastructure (NCI) and Multi-modal Australian Sciences Imaging and Visualisation Environment (MASSIVE) facilities through the National Computational Merit Allocation Scheme supported by the Australian Government.

REFERENCES

Amili, O. 2012 Measuring the wall shear stress in wall-bounded turbulence. PhD thesis, Monash University, Australia.

Amili, O. & Soria, J. 2011 A film-based wall shear stress sensor for wall-bounded turbulent flows. *Exp Fluids* **51** (1), 137–147.

Bakewell, H. P. & Lumley, J. L. 1967 Viscous sublayer and adjacent wall region in turbulent pipe flow. *Phys Fluids* **10** (9), 1880–1889.

Grosse, S. & Schröder, W. 2009 Wall-shear stress patterns of coherent structures in turbulent duct flow. *J Fluid Mech* **633**, 147–158.

Hama, F. R. 1954 Boundary-layer characteristics for smooth and rough surfaces. *Trans Soc Nav Arch Mar Eng* **62**, 233255.

Haritonidis, J. H. 1989 The measurement of wall shear stress. *Adv Fluid Mech* pp. 229–261.

Kline, S.J., Reynolds, W.C., Schraub, F.A. & Runstadl, P.W. 1967 Structure of turbulent boundary layers. *J Fluid Mech* **30** (pt 4), 741–773.

Mizuno, Y., Atkinson, C. & Soria, J. 2011 Topology and dynamics of flow structures in wall-bounded turbulent flows. *15th European Turbulence Conference, Sep 2011, Warsaw, Poland* .

Sheng, J., Malkiel, E. & Katz, J. 2009 Buffer layer structures associated with extreme wall stress events in a smooth wall turbulent boundary layer. *J Fluid Mech* **633**, 17–60.

Simens, M. P., Jiménez, J., Hoyas, S. & Mizuno, Y. 2009 A high-resolution code for turbulent boundary layers. *J Comput Phys* **228** (11), 4218–4231.

Tomkins, C. D. & Adrian, R. J. 2003 Spanwise structure and scale growth in turbulent boundary layers. *J Fluid Mech* (490), 37–74.